Applied Catalysis B: Environmental 226 (2018) 258–268

Contents lists available at ScienceDirect

Applied Catalysis B: Environmental

journal homepage: www.elsevier.com/locate/apcatb

Chemical looping steam reforming of acetic acid in a packed bed reactor

Oluwafemi A. Omoniyi*, Valerie Dupont

School of Chemical and Process Engineering, University of Leeds, LS2 9JT, UK

ARTICLE INFO

Keywords:
Chemical looping
Steam reforming
Acetic acid
Nickel
Hydrogen production

ABSTRACT

Chemical looping steam reforming of acetic acid (CLSR-HAc) was carried out in a packed bed reactor at 650 °C and 1 atm using two nickel-based catalysts ('A' with alumina support and 'B' with calcium aluminate support) to study the effect of the temperature of oxidation (T_{OX}) on the efficiency of the process and the materials properties of the catalysts upon cycling. CLSR-HAc could not be sustained with steady outputs with T_{OX} of 600 °C for catalyst A, but it was conducted successfully at temperatures up to 800 °C, whereas with B it could be operated reaching close to equilibrium conditions over five cycles with T_{OX} of 600 °C. CLSR-HAc can run efficiently for further cycles at the right operating conditions (S/C of 3, WHSV of 2.5 h^{-1}, T_{OX} 800 °C, T_{SR} 650 °C) even in the presence of the side reactions of acetic acid decomposition and coking. The yield of hydrogen produced had a minimum efficiency of 89% compared to equilibrium values, and the acetic acid conversion was in excess of 95% across 10 chemical looping steam reforming cycles. High purity hydrogen (> 90% compared to equilibrium values) was also produced in this study. Chemigrams obtained from TGA-FTIR analysis indicates that two forms of carbon were formed on the catalyst during CLSR-HAc; TEM images and diffraction patterns indicate that poly graphitic carbon and amorphous carbon were formed while SEM images of the oxidised catalyst showed that the carbon was eliminated during the oxidation step of CLSR. A full carbon elemental balance of the process confers that majority of the carbon share (ca 90%) was utilised for efficient steam reforming of acetic acid with ca 10% of the carbon input deposited during the reduction step and subsequently burned during oxidation over the CLSR cycles.

1. Introduction

Hydrogen is a gas utilised in many industries globally; it has a global market share of over 40 million dollars which is expected to increase exponentially to over 180 billion dollars as its demand increases [1]. The significant increase in its demand is notably due to its high utilisation in industrial applications particularly fertiliser industries, oil refining and petrochemical industries, food processing, metallurgical processes [1–3], and increasingly due to the growth of fuel cell technologies. The environmental benefits in regards to its low carbon footprint when utilised potentially as an energy vector are mitigated by the fact that 96% of hydrogen consumed globally is produced from conventional fossil fuels which has prompted vast research on the utilisation of renewable resources for the production of hydrogen.

Biomass resources for H_2 production have advantages over intermittent renewables like wind and solar in that they are abundant globally, provide a natural storage medium, and because they can be harnessed easily [4–6]. The production of hydrogen from biomass can be done through different routes, however; a promising route is an indirect method which involves the fast pyrolysis of the biomass residue to bio-oil first before its conversion to hydrogen [7]. This method offers advantages to direct gasification methods on several fronts. Firstly, unlike many gasification processes, pyrolysis avoids the formation of heavy tars and thus can have a lower burden of clean-up and maintenance. Secondly, pyrolysis oils can be used for other purposes, particularly as additives in refining or as feedstock for the production of valuable chemicals. Pyrolysis also requires milder temperatures than gasification, making the process less prone to the energy inefficiencies

Abbreviations: CLSR, chemical looping steam reforming; HAc, acetic acid; T_{OX}, temperature of oxidation; T_{SR}, temperature of steam reforming; TGA-FTIR, thermogravimetric analysis coupled to Fourier transform infrared spectroscopy; TEM and SEM, transmission electron microscope and scanning electron microscope; X_{HAc} and X_{H2O}, conversion fraction of acetic acid and water respectively; $\dot{n}_{out,dry}$, total molar flow rate dry basis; n_i, number of moles of specie i; y_i and y_a, molar fraction of specie i and all gases in the outlet gas respectively; Sel_i, selectivity of individual constituent; W_i, molar weight of specie i; $\dot{n}_{i,in}$ and $\dot{n}_{i,out}$, molar flow rate in and out of specie I respectively; n_{Cgas}, number of moles of carbon gasified in air feed stage; $n_{Ni,t}$ and $n_{Ni(i)}$, number of moles of nickel oxidised and number of moles of nickel in catalyst; ($\dot{n}_{Ni\rightarrow NiO}$) and ($\dot{n}_{c,gas}$), rates of nickel oxidation of the reduced catalyst and rate of carbon gasified, respectively; $X_{Ni\rightarrow NiO}$, X_{C-gas}, extent of nickel and carbon oxidation; OC, oxygen carrier; sccm, standard cubic centimeters per minute; cc/g, cubic centimetre per gram; CHNS, carbon, hydrogen and nitrogen elemental analysis; BET, Brunauer–Emmett–Teller method; ICP-MS, inductively coupled plasma mass spectrometry; TOC, total organic carbon; S/C, steam to carbon ratio

* Corresponding author.
E-mail addresses: pmoao@leeds.ac.uk (O.A. Omoniyi), v.Dupont@leeds.ac.uk (V. Dupont).

https://doi.org/10.1016/j.apcatb.2017.12.027
Received 18 July 2017; Received in revised form 6 December 2017; Accepted 11 December 2017
Available online 16 December 2017
0926-3373/ © 2018 The Authors. Published by Elsevier B.V. This is an open access article under the CC BY license (http://creativecommons.org/licenses/BY/4.0/).

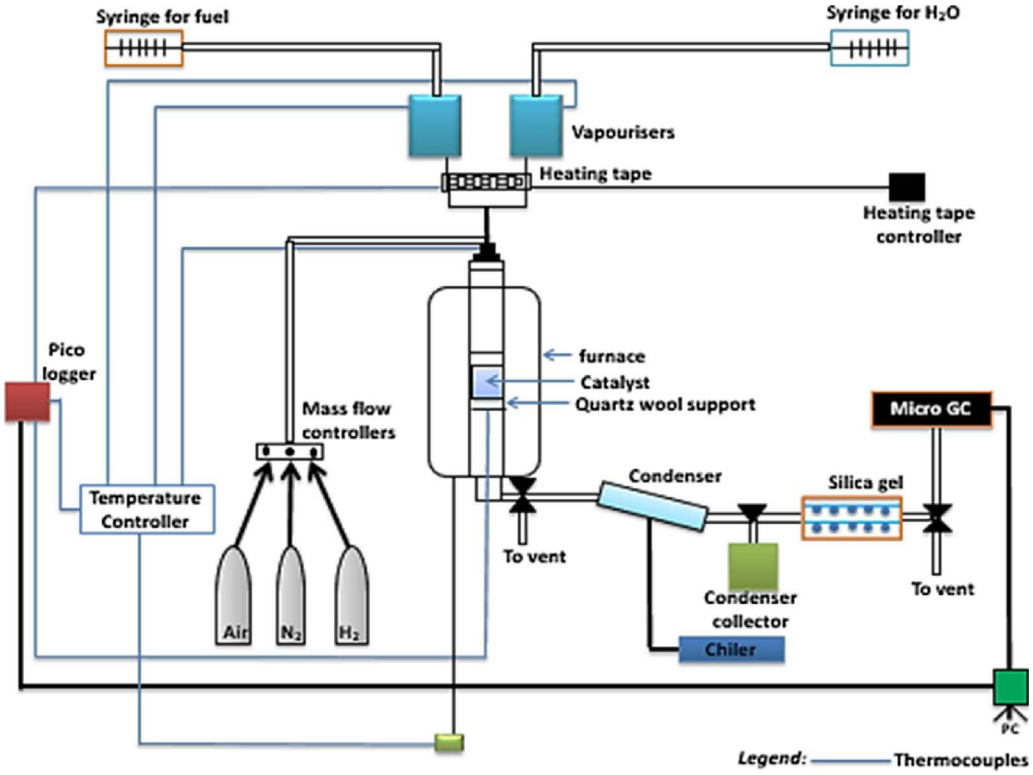

Fig. 1. Reactor set-up for evaluation of the CLSR-HAc cycles.

associated with the irreversibilities caused by large temperature gradients in the system. Finally, pyrolysis operates at lower pressure, thus safer, conditions. Bio-oils are chemically complex and rather unstable mixtures which has prompted the study on the utilisation of aqueous fractions of pyrolysis oils, model compounds or mixtures and oxygenates for pilot scale research and studies [8–15].

Acetic acid is one of the most studied model compound of pyrolysis oils for the production of hydrogen; this is due to its dominant presence in most bio-oil compositions [16,17]. Its thermal conversion to hydrogen, however, has been characterised with challenges due to side reactions and formation of intermediates particularly on the surface of the catalyst [9]. These have increased the need for process intensification and optimisation measures with the view of reducing some of the downsides encountered, as well as reducing the energy cost of the process.

The conventional process of steam reforming of acetic acid to hydrogen has been well researched [9,12,18–20]. Basagiannis and Verykios concluded that the reforming of acetic acid is complicated due to side reactions prominent at lower reforming temperatures, they also stipulated that the rate of carbon deposition observed on the catalyst is generally determined on the reforming temperature, catalyst utilised and the feed to steam ratio [21].

Process intensification measures particularly chemical looping steam reforming (CLSR) has been promoted to ease the challenges observed in the steam reforming process [22]; CLSR utilises an 'oxygen transfer material' (OTM) also known as 'oxygen carrier' (OC) which drives the reactions in a cyclic process as follows. As the steam reforming reactions are very endothermic, heat is provided at the heart of the process by the oxidation reactions in the reactor under air feed [23]. This ensures no dilution of the reformate mix product with diluent N_2 when the feed flow is switched to fuel feed and steam, some of fuel being sacrificed first to reduce the OC and thus activate it as a catalyst of the steam reforming and water gas shift reactions. The use of external burners to heat up the reformer and the costs associated with the use of highly corrosion resistant materials and combustion control techniques are thus avoided, while the absence of large temperature gradients during heat transfer reduces process irreversibilities and thus increases thermodynamic efficiency. The OC catalyst as utilised in this study should nevertheless have suitable characteristics particularly a high resistance to attrition, agglomeration and carbon deposition [24,25].

Previous reported works on the CLSR of acetic acid and other liquids of biomass origin have been centred on the reactivity of the catalyst across the looping cycles; it has been reported that the fuel conversion and consequently hydrogen yield reduces upon cycling for the CLSR of bio-diesel and scrap tyre pyrolysis oils [23,26]. Other studies indicated that no deterioration occurs in fuel conversion and hydrogen yield from the CLSR of other liquids of biomass origins investigated [27–29]. Thus, the efficiency of the fuel conversion and hydrogen yield of CLSR is influenced by the feedstock and operating conditions utilised, and the deterioration of the reactivity of the catalyst is generally due to carbon deposition, sintering and thermal decomposition of the feedstock.

This paper studies the redox cycling ability and process efficiency of chemical looping steam reforming of acetic acid (CLSR-HAc) in a packed bed reactor; ten experimental cycles were performed using the experimental approach as described in the next section. The auto-reduction activity of acetic acid of one of the nickel catalyst utilised in the present study has been previously investigated and it has been established that acetic acid performs considerably well when compared to the same catalyst after reduction by hydrogen [30]. The process outputs, hydrogen yield, conversion and selectivity to carbon gases for each cycle and two OC catalysts were compared with the view to measure consistency across the cycles; and characterisation of the catalysts was also done post-experimentally to ascertain any changes in morphology. The effect of the oxidation temperature on the reforming process was examined to ascertain its influence on the reforming process and full carbon balances were conducted to evaluate the share of solid carbon by-product during the process.

2. Experimental approach and methods

2.1. Materials and reactor set-up

Two commercial Nickel-based catalysts were used in this study and were supplied by TST limited; Catalyst A contained 18 wt.% NiO on alpha-alumina support while Catalyst B contained 15 wt.% NiO on calcium aluminate support. Both catalysts were supplied as pellets but were crushed and sieved to 250–350 μm before utilisation. Acetic acid utilised for the experiments was purchased from Sigma-Aldrich (≥99%) and distilled water was used for all experiments.

The reactor system utilised in this study, as depicted in Fig. 1, is a down flow system using a fully insulated packed bed reactor consisting of a stainless-steel tube of 12.7 mm internal diameter and 25 cm length. The reactor was connected to two 180 mm long aluminium and stainless steel vaporisers; the vaporisers were used to preheat the acetic acid fuel and the water co-reactant separately before they were introduced into the reactor. For all experimental runs, the pre-heat temperatures were set at 50 °C and 150 °C for acetic acid pre-heat and water vaporisation respectively, this was done to prevent or minimise acetic acid decomposition and induce full water vaporisation. The temperatures of the vaporisers and the furnace were controlled by a temperature PID controller while a Pico Log was used to monitor and identify any heat loss in the system. The flow rates of water and acetic acid were controlled by two separate programmable New Era syringe pumps while the flow of gasses into the system (air, H_2, N_2) were regulated by mass flow controllers supplied by MKS. The product gas composition were detected and measured by a Micro gas chromatograph (Micro-GC, Varian) after the effluents passed through a condenser and a moisture trap; the Micro-GC consisted of two columns, the first which operated with a back flush was a molecular sieve 5A column and was used to detect H_2, O_2, CO, N_2, while the second was a Pora Plot Q column used to detect CO_2 and CH_4 as well as C_2 and C_3 gases.

2.2. Experimental procedures

Chemical looping steam reforming (CLSR) consists of two basic steps; the reducing/reforming step (fuel-steam feed) and the oxidation step (air feed). Both steps as carried out in this study are preceded by purging the reactor system with N_2 (200 sccm) and raising the temperature of the furnace to the required temperature for each step. The flow rates of acetic acid and water in the reducing step were set to 0.978 ml/h and 1.846 ml/h respectively and N_2 (27 sccm for experiments with WHSV set to 1.18 h^{-1} and 31 sccm for experiments with WHSV set to 2.5 h^{-1}) were also utilised in all reforming steps. The reducing/reforming step was carried out at two temperatures: 600 °C and 650 °C, and at steam to carbon ratio 3 using 2 g of either Catalyst A or Catalyst B. This is because previous studies on pyrolysis oils and their model compounds indicated that the reforming process is optimal in this range [15,30–33].

The global reactions that are expected to occur in the reducing/reforming step are summarised and expressed as follows in Reactions (R1) and (R2);

$$C_2H_4O_2 + 4NiO \rightarrow 2CO_2 + 2H_2O + 4Ni \quad (R1)$$

$$C_2H_4O_2 + 2H_2O \xrightarrow{Ni} 2CO_2 + 4H_2 \quad (R2)$$

This includes the auto-reduction of the catalyst by acetic acid (Reaction (R1)) and complete steam reforming of acetic acid (Reaction (R2)). The sequence of reactions for the reducing phase is, however, more complex than what is described in Reactions (R1) and (R2) as other intermediate and side reactions might occur. Intermediate reactions might include NiO reduction by CO, H_2 and other hydrocarbon intermediates, side reactions include coking, formation and dissociation of intermediates, decomposition of acetic acid, ketonisation and sometimes methanation reactions, and water gas shift [30].

The reducing step for the runs in this study was carried out for 2 h using 2 g of the catalyst. The catalyst as prepared into granules is first reduced or activated by 5% H_2/N_2 (Reaction (R3)) at the temperature set for the reducing step. Auto-reduction of the catalyst by acetic acid in subsequent cycles is also carried out after the oxidation step at the temperature set for the reducing step; this is ≥550 °C for all experimental runs and has been reported to be adequate for full reduction of Ni-based catalysts by acetic acid [34].

$$NiO + H_2 \rightarrow Ni + H_2O \quad (R3)$$

The oxidation step was done at temperatures ranging between 600 °C and 800 °C with the view to evaluate the effect of the oxidation temperature (T_{OX}) on the overall process. Air was passed through the reactor to re-oxidise the already utilised catalysts from the reducing/reforming step while also gasifying carbon formed on the catalyst from the preceding fuel feed stage. The main reactions occurring are summarised in reactions (R4)–(R6) and the air feed during the oxidation step was allowed to run until the concentration of oxygen detected in the micro-GC stabilised at 21 Vol%.

$$2Ni + O_2 \rightarrow 2NiO \quad (R4)$$

$$C + O_2 \rightarrow CO_2 \quad (R5)$$

$$2C + O_2 \rightarrow 2CO \quad (R6)$$

2.3. Solids and condensates characterisation

Characterisation work was also carried out on the used catalyst and collected condensate to analyse the amounts of carbon and hydrogen deposited over cycles and observe any changes in morphology after chemical looping steam reforming. The carbon content on the utilised catalyst was determined using CHNS elemental analysis conducted in a Flash EA 2000 elemental analyser. BET analysis was conducted using a Quantachrome Nova 2200e instrument to observe any changes in the open porosity and surface area of the used catalyst. SEM-EDX was conducted using a high-resolution Hitachi SU8230 and Carl Zeiss EVO MA15 both coupled with an Oxford Instruments Aztec Energy EDX system, and TEM images was derived using a FEI Tecnai TF20. The SEM-EDX and TEM were carried out for surface topology analysis and solid carbon product distribution. TGA-FTIR was also conducted using a Stanton-Redcroft TGA connected to a FTIR (Nicolet iS10, Thermo scientific) to observe the mass loss and predict the type of carbon produced using the CO_2 chemigram observed. ICP-MS was conducted on the collected condensate using a SCIEX Elan 900 by Perkin Elmer and TOC tests were also conducted on the collected condensate using a Hach-Lange IL 550 analyser (differential method) to check for possible leaching of the catalyst and calculate the carbon content in the condensate respectively.

2.4. Process outputs and material balances

Balances of the N, C, H and O elements during the fuel-steam feed stage and the air feed stage were used to determine in turn the reactants conversion to gas products, yield of hydrogen, while the gas compositions determined the selectivity to carbon-containing gases as described in [28,30,35]. A nitrogen balance was used to calculate the total molar gas output flow rate ($\dot{n}_{out,dry}$) using the feed molar rate of N_2 and the molar fraction of N_2 detected by the micro GC ($\dot{n}_{out,dry} = \dot{n_{N_2,in}}/y_{N_2}$). This in turn was used to calculate the conversion of the reactants in the fuel-steam feed stage; acetic acid conversion to gas products in the fuel feed stage is calculated from a carbon balance as summarised in Eq. (1A) while the water conversion (Eq. (1B)) is calculated from a hydrogen balance;

Eqs. (1A) and (1B) Conversion (fuel and water)

$$\boldsymbol{X_{HAc}}(\%) = 100 \times \frac{(\dot{n}_{\boldsymbol{out,dry}} \times (\boldsymbol{y}_{CO} + \boldsymbol{y}_{CO_2} + \boldsymbol{y}_{CH_4} + 2\boldsymbol{y}C_2H_6 + 2\boldsymbol{y}C_2H_4 + 3\boldsymbol{y}C_3H_6 + 3\boldsymbol{y}C_3H_8))}{2 \times \boldsymbol{n_{HAC,in}}} \quad (1A)$$

$$\boldsymbol{X}_{H_2O}(\%) = 100 \times \frac{(\dot{n}_{\boldsymbol{out,dry}} \times (\boldsymbol{y}_{H_2} + 2\boldsymbol{y}_{CH_4} + 3\boldsymbol{y}_{C_2H_6} + 2\boldsymbol{y}_{C_2H_4} + 3\boldsymbol{y}_{C_3H_6} + 4\boldsymbol{y}_{C_3H_8}) - 2 \times \boldsymbol{n_{HAC,in}} \times \boldsymbol{X_{HAc}})}{\boldsymbol{n}_{H_2O,in}} \quad (1B)$$

The calculation of the acetic acid conversion to gases did not represent the conversions to solid carbon or organic condensates, which were evaluated separately by CHNS analysis of the used catalyst and TOC analysis of the condensates after the experiments in order to close the carbon balance over full cycles of reduction/steam reforming stages under acetic acid and steam feed, alternating with the oxidation stage under air feed. A value of X_{HAc} during HAc/steam feed lower than 100% denoted carbon deposition on the catalyst or in the condensate. The hydrogen yield (wt.%) under HAc/steam feed is defined as a ratio of the weight of hydrogen in the process output to the weight of acetic acid feedstock (no water) (Eq. (2)). According to stoichiometry of reaction (R3), the maximum theoretical hydrogen yield is 13.45 wt%. The hydrogen purity dry basis (%) was also calculated as indicated in Eq. (3); the water conversion, hydrogen yield and hydrogen purity is compared with chemical equilibrium and stoichiometric values to ascertain the efficiency of the fuel-water feed stage.

Eq. (2) Hydrogen yield (wt.%)

$$\textbf{Hydrogen yield (wt. \%)} = \frac{\boldsymbol{W}_{H_2} \times 100 \times \dot{n}_{\boldsymbol{out,dry}} \times \boldsymbol{y}_{H_2}}{\boldsymbol{W_{HAC}} \times \boldsymbol{n_{HAC,in}}} = \frac{2 \times 1.01 \times 100 \times \dot{n}_{\boldsymbol{out,dry}} \times \boldsymbol{y}_{H_2}}{\boldsymbol{n_{HAC,in}} \times \boldsymbol{W_{HAC,dry}}} \quad (2)$$

Eq. (3) Hydrogen Purity (% Dry basis)

$$\textbf{Hydrogen Purity (\% Dry basis)} = \frac{\textbf{moles of hydrogen detected in process gas output}}{\textbf{total gas moles detected} - \textbf{moles of } N_2} \times 100 \quad (3)$$

Selectivity to carbon gases and hydrogen gases was also calculated as described in Eqs. (4) and (5) respectively;

Eq. (4) Selectivity to C-gases

$$sel_{i,C}\% = 100 \times \frac{\alpha_i y_{i,C}}{\sum_j^n \alpha_{j,C} y_{j,C}} \quad (4)$$

Where indices α_i and α_j represent the carbon atom number of the relevant carbon gas species.

Eq. (5) Selectivity to H_2-gases

$$sel_{i,H_2}\% = 100 \times \frac{\alpha_i y_{i,H_2}}{\sum_j^n \alpha_{j,H_2} y_{j,H_2}} \quad (5)$$

Where indices α_i and α_j represent the hydrogen atom number of the relevant hydrogen gas species.

In the oxidation step, the calculated molar flow rate ($\dot{n}_{out,dry}$) realised from nitrogen balance was used to calculate the rate of oxidation of the reduced catalyst ($\dot{n}_{Ni \rightarrow NiO}$) and carbon deposited from the prior steam reforming phase ($\dot{n}_{c,gas}$) using an oxygen balance and carbon balance respectively as detailed in Eq. (6); the integration of the calculated rate over time gave the total number of moles of nickel oxidised ($n_{Ni,t}$) and carbon gasified (n_{Cgas}) in the oxidation step respectively.

Eq. (6) Rate of oxidation of reduced nickel catalyst and Carbon gasified

$$(\dot{n}_{Ni \rightarrow NiO}) = 2\dot{n}_{O_2,\boldsymbol{in}} - \dot{n}_{\boldsymbol{out,dry}} \times (2\boldsymbol{y}_{O_2} + \boldsymbol{y}_{CO} + 2\boldsymbol{y}_{CO_2})$$
$$(\dot{n}_{\boldsymbol{c,gas}}) = \dot{n}_{\boldsymbol{out,dry}} \times (\boldsymbol{y}_{CO} + \boldsymbol{y}_{CO_2}) \quad (6)$$

The calculated $n_{Ni,t}$ was used for the calculation of the extent of nickel conversion using Eq. (7) while the n_{Cgas} was essential for ascertaining the overall carbon balance of the process and extrapolating the extent of carbon gasified (number of moles of carbon gasified at a time with respect to the total number of moles gasified at the air feed stage);

Eq. (7) Extent of Nickel Oxidation

$$\boldsymbol{X}_{Ni \rightarrow NiO}(\%) = \frac{\boldsymbol{n}_{Ni,\boldsymbol{t}}}{\boldsymbol{n}_{Ni(\boldsymbol{i})}} \times 100 \quad (7)$$

Chemical equilibrium calculations for the parameters considered were determined using values obtained from the Chemical Equilibrium with Applications (CEA) software [36]. The software was used to derive equilibrium values for the process output using the set conditions for the experimental runs (P = 1 bar, T = 600 °C, 650 °C, Omit = C(gr), H_2O(cr) H_2O(l)). These process outputs were in turn used to calculate the process outputs at equilibrium using Eqs. (1A), (1B), and (4) by replacing the relevant molar flow rates in the reactor with just molar outputs predicted at equilibrium at same conditions.

3. Results and discussion

3.1. Process outputs with time on stream and upon redox cycling of CLSR-HAc

The gases detected by the micro-GC for all experimental runs in this study were CO, CO_2, CH_4, C_2H_6, C_3H_8, (the last two always remaining below threshold of detection), H_2, N_2, and O_2 (observed during the oxidation steps). In the event of acetone being a significant product of the process, it would have been detected by significant C content in the condensates. Ketonisation reactions are generally inhibited by nickel catalysts and are stipulated to occur during the reforming of acetic acid ideally at temperatures below 600 °C [37,38].

3.1.1. Process outputs with time on stream- fuel-water feed stage

The fuel-steam feed stage as described in 2.2, was carried out at 600 °C and 650 °C for all experimental runs in this study. A similar trend for the main output gas species molar fractions with time on stream was observed for the first cycle (H_2 reduced catalyst) and subsequent cycles (auto-reduced) for the experimental runs as shown in Fig. 2 for catalyst B (T_{SR} = 600 °C, T_{OX} = 600 °C, S/C = 3, WHSV = 2.5 h^{-1}).

In the H_2 reduced cycle, CO is detected ca. 500 s earlier than CO_2 whereas, in the auto-reduced cycle, CO and CO_2 are simultaneously detected. Similarly, the lag between H_2 and CO generation is increased by 250 s for the auto-reduced cycle. This is consistent with a steam reforming reaction delayed by the consumption of the fuel to carry out the reduction of the nickel oxide to metallic nickel, with the steam reactant exhibiting temporary faster reactivity for dissociation to hydrogen on the reduced catalyst compared to the hydrocarbon reducing reactions and steam reforming.This has also been observed in previous studies where a short lag period or simultaneous partial auto reduction and reforming reactions are observed [27,30]. A similar dry outlet gas composition profile was derived for the H_2 reduced cycle and auto reduced cycle when catalyst A was utilised with a slight increase in the lag (50 s–200 s) between CO and H_2 generation in the auto reduced cycle.

3.1.2. Process gas output (Oxidation phase) and extent of oxidation

The oxidation phase in this study was carried out between 600 °C and 800 °C by passing air through the reactor. An increase of approximately 30–50 °C was observed at the beginning of all oxidation phase runs; this was due to the exothermic nature of the oxidation reactions.

The operating conditions at which the oxidation phase is conducted has an effect on the overall process efficiency; it is also fitting to check

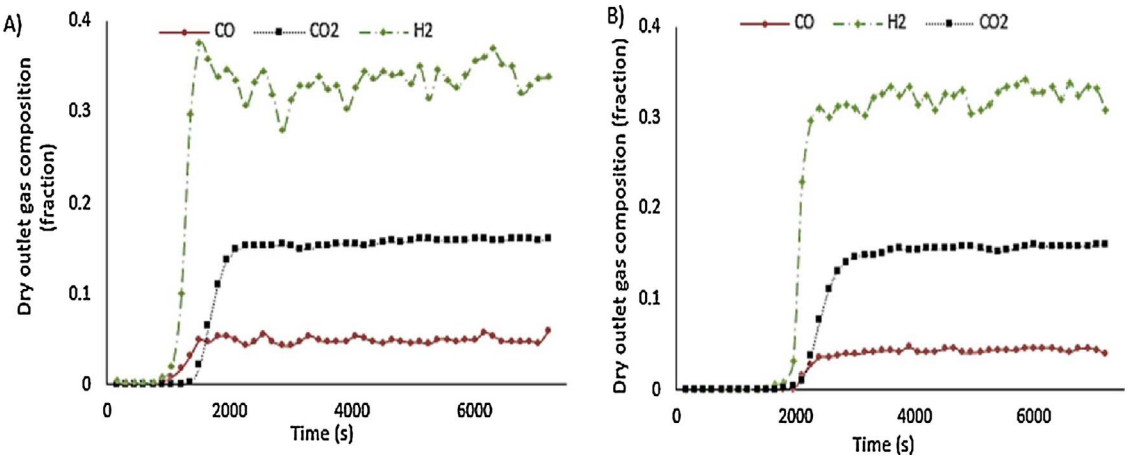

Fig. 2. Dry outlet gas composition of products after reforming at (A) cycle one where the catalyst has been activated by reduction with hydrogen (b) Auto reduced catalyst (i.e. catalyst reduced with acetic acid) at the 5th reduction run (T_{SR} = 600 °C, T_{OX} = 600 °C, catalyst B, WHSV = 2.5 h^{-1}, S/C = 3).

the extent of oxidation of nickel during the air feed stage with the view to ascertain the effectiveness of the air feed stage. Five CLSR cycles (4 oxidation phase runs) were conducted on catalyst B at WHSV 1.18 h^{-1} and at S/C of 3 to check the oxidation effectiveness. Air was passed at 200 sccm and 2 g of inert material (sand) were mixed with catalyst B (2 g) in the reactor load. The oxidation temperature (T_{OX}) under air feed was also set at 800 °C while the reducing-steam reforming stage under acetic acid/steam feed was carried out at 650 °C.

The process gas composition detected by the micro GC for all oxidation runs under air feed contained oxygen, nitrogen, CO and CO_2 as depicted in Fig. 3. The CO and CO_2 indicate the oxygen passed through air was utilised in oxidation of carbon that had been formed during the preceding fuel-steam feed stage; it is also expected as reported in several literature on CLSR that the catalyst is oxidised from its catalytically active nickel state to deactivated nickel oxide (reaction (R4)) [30,35].

Review of the literature indicates that the oxidation of carbon may occur first before the diffusion controlled nickel oxidation [35,39]; however, it was observed in this study that both reactions occurred in parallel with carbon oxidation starting first and freeing up space on the nickel catalyst which is then oxidised whilst more carbon is burnt off.

Integrating the rates of the nickel oxidation ($\dot{n}_{Ni\rightarrow NiO}$) over time allows to determine whether the nickel redox extent ($X_{Ni\rightarrow NiO}$) calculated using Eq. (7) is maintained at the same level from cycle to cycle.

The number of moles of nickel oxidised at steady oxygen output

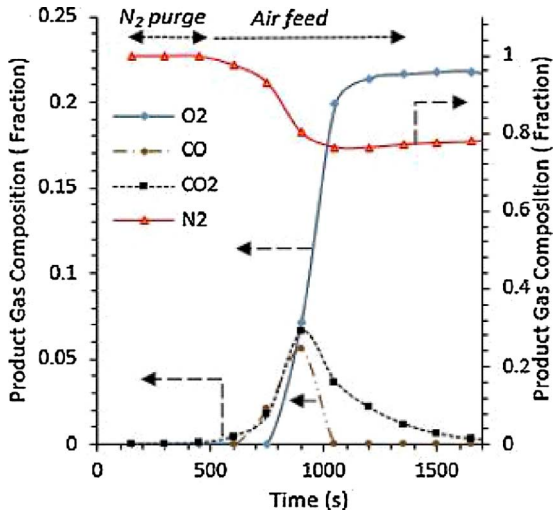

Fig. 3. Product gas composition (mol fractions) for oxidation step at T_{SR} = 650 °C, T_{OX} = 800 °C, catalyst B, WHSV = 1.18 h^{-1}, S/C = 3, A).

Table 1
Nickel oxidised in CLSR oxidation phase (T_{SR} = 650 °C, T_{OX} = 800 °C, catalyst B, WHSV = 1.18 h^{-1}, S/C = 3).

	$\dot{n}_{Ni\rightarrow NiO}$(mol/s)	$n_{Ni,t}$ (mol)	$X_{Ni\rightarrow NiO}$ (%) (Eq. (7))	Duration of Ni Oxidation (s)
1	8.98×10^{-6}	4.03×10^{-3}	100.22	449
2	5.99×10^{-6}	3.80×10^{-3}	94.63	634
3	5.83×10^{-6}	3.25×10^{-3}	80.83	557
4	6.29×10^{-6}	3.37×10^{-3}	83.97	536

(evidencing the end of oxidation reactions) is shown in Table 1. There is a drop in the extent of nickel oxidised from the first oxidation cycle to subsequent oxidation cycles. However, the extent of nickel oxidation remained > 80% across the other cycles; this indicates that the oxidation of nickel can be maintained across the oxidation cycles.

3.1.3. Overall carbon balance of CLSR process

An overall carbon balance was carried out on the CLSR process (using the set operating conditions as descibed in 3.1.2) as detailed in Table 2. < 5% of the carbon calculated through the carbon balance was unaccounted for in the overall process across 5 cycles, indicating high accuracy of the carbon balance and distribution across products for the 5 cycles, as well as validating the methodology for their calculation.

The carbon distribution in the products across the process cycles indicates the major share of carbon was in the process gas (85%–92%) and as a solid on the oxidised catalyst (7%–14%) across all cycles, where n_{Cgas} represented deposited solid carbon from the previous cycle; these entail that most of the carbon in the feedstock was utilised in the process for auto-reduction and steam reforming, whilst approximately 10% was deposited on the catalyst; it is essential to stress that the amount deposited on the catalyst must have been influenced by the presence of catalytically inactive material in the reactor load. Carbon in the condensates was negligible in all the cases.

3.2. Effect of oxidation temperature on process outputs

The effect of T_{OX} on chemical looping steam reforming was investigated by oxidising the used reforming catalyst (catalyst A) at 600 °C, 700 °C, and 800 °C. T_{SR} was kept at 600 °C and the experiments were carried out at S/C of 3 and WHSV of 2.36 h^{-1}. The effect of the catalyst utilised was also investigated by performing 5 reforming experimental cycles using catalyst B at the same operating conditions but oxidising only at 600 °C.

Table 2
Overall Carbon balance of CLSR process (T_{SR} = 650 °C, T_{OX} = 800 °C, catalyst B, WHSV = 1.18 h^{-1}, S/C = 3).

	C in feed (mol) during HAc/steam feed	X_{HAc} (%) (Eqs. (1A) and (1B))	C product during HAc/ steam feed (mol)	n_{Cgas} (mol) (Eq. (6))	C in the condensate (mol)	Total carbon (gas + solid + condensate) (mol)
1	6.82×10^{-2}	93.1	6.35×10^{-2}	5.04×10^{-3}	1.99×10^{-5}	6.86×10^{-2}
2	6.82×10^{-2}	85.9	5.86×10^{-2}	6.19×10^{-3}	4.48×10^{-5}	6.49×10^{-2}
3	6.82×10^{-2}	85.7	5.86×10^{-2}	9.64×10^{-3}	3.39×10^{-5}	6.83×10^{-2}
4	6.82×10^{-2}	91.8	6.26×10^{-2}	7.19×10^{-3}	1.39×10^{-5}	6.98×10^{-2}
5	6.82×10^{-2}	84.5	5.76×10^{-2}	7.91×10^{-3}	0.10×10^{-5}	6.55×10^{-2}

3.2.1. Gas outputs in oxidation temperature study

Both catalysts behaved similarly and efficiently during steam reforming with hydrogen yield efficiency > 83%, hydrogen purity efficiency > 97%, water conversion efficiency > 75% and fuel conversion efficiency > 89% when compared to equilibrium values. The high efficiency did not persist to the 2nd chemical looping reforming cycle after oxidation was carried out at 600 °C for catalyst A, as sustained reforming could not be maintained over the duration observed. This was not the case with catalyst B, as sustained production of hydrogen with high efficiency was observed over five cycles of CLSR with T_{Ox} set to 600 °C. The lack of sustained steam reforming in the second cycle of reforming for catalyst A is due to increased coking via thermal decomposition (shown in the carbon balances); Coking might have been enhanced by the acidic nature of the catalyst support in Catalyst A [21,40,41]. Acidic catalysts support increases the chances of thermal decomposition and other polymerisation reactions resulting in graphitic carbon decomposition on the acidic sites of the support [21].

Sustained steam reforming was observed during the CLSR of acetic acid using catalyst A after oxidising at higher temperatures (700 °C and 800 °C) while leaving the temperature at the reducing phase at 600 °C over five cycles (Table 3) Fig. 4 shows the conversion fraction, selectivity to C gases, hydrogen yield and purity obtained for the duration of the steam reforming phase using the auto reduced catalsyt A at the second cycle at T_{OX} set to 700 °C. A similar profile to Fig. 4 was obtained for other cycles at T_{OX} set to 700 °C or 800 °C. More than 89% of the fuel was converted across all five cycles of CLSR when T_{OX} was set at 700 °C or 800 °C, corresponding to a water conversion efficiency > 73% across all the cycles. This also corresponded to hydrogen yield efficiencies > 71% and > 82% when compared to equilibrium and stoichiometric values respectively. High hydrogen purity efficiencies (> 97% when compared to equilibrium values and > 91% when compared to stoichiometric calculations) were achieved across all CLSR experimental runs as shown in Table 3.

Thus, T_{OX} has a bearing effect on the process stability at the subsequent auto-reduction and steam reforming run as seen in catalyst A; however, the catalyst support in the catalyst utilised for the CLSR process is also essential.

3.2.2. Solid carbon product in T_{OX} study

There is an obvious decline in the carbon content (mol) of catalyst A as T_{OX} of catalyst A is increased as shown in Table 4; with a 68% decrease in carbon content (mol) found for catalyst A when oxidised at 800 °C compared to 600 °C. There is also a large difference in the carbon content (mol) when catalyst A and catalyst B are compared; the carbon present in catalyst A is much higher than that observed in catalyst B when oxidised at 600 °C (57% increase). CHN analysis of used CLSR catalyst A after five cycles of CLSR also exhibits a higher carbon content when compared to the corresponding carbon content for catalyst B as seen in Table 4.

The increase in T_{OX} alone does not alleviate all challenges highlighted in catalyst A because incomplete gasification of the carbon deposited in the acidic sites might subsequently occur during the oxidation stage, which would prompt further gasification required in the next reforming or reducing cycle. This phenomenon would affect the efficiency of the CLSR process as the potential of thermal decomposition and cracking reactions might increase particularly at the beginning of the reducing phase where auto-reduction or dominant auto-reduction plus suppressed steam reforming are occurring [29,30].

The presence of an alkali support as in the case of catalyst B has been shown to improve the stability and selectivity of steam reforming catalysts [42]; they are promoted to increase the reforming process by enhancing water gas shift and catalyst reduction [43]. It has also been reported that catalysts with less acidic supports such as catalyst B would have a higher ability to promote gasification and complete oxidation of deposited carbon, and hence promotes a better efficiency for auto-reduction and reforming in subsequent reducing phase [44].

3.2.3. Catalysts characteristics after CLSR-HAc use in T_{OX} study

Surface area analysis of the catalysts is also important as it has been associated with the efficiency of the reforming process; the surface area analysis of CLSR is difficult to elucidate due to the several reactions occurring at the same time, it has been reported that the reduced catalyst (after reforming in a looping cycle) would have a higher surface area than its subsequent oxidised form [23,26]. The increase in the surface area and pore volume in the reduced catalysts is due to the formation of smaller pores caused by openings of the pore mouths plugged with the oxidised form of the catalyst and/or the different molar volume of the Ni particle when compared to its oxidised form. Table 5 details results from the BET analysis of catalyst B before and after CLSR (5 cycles, S/C = 3, T_{SR} = 600 °C, WHSV = 2.5 h^{-1}); a loss of

Table 3
Conversion fraction, purity and hydrogen yield over 5 cycles (T_{SR} = 600 °C, WHSV set to 2.36 h^{-1}, and S/C = 3).

	Cycle	X_{HAc} (fraction) (Eqs. (1A) and (1B))			X_{H_2O} (fraction)			Hydrogen purity (%) (Eq. (3))			Hydrogen yield (wt.%) (Eq. (2))		
T_{OX} (°C)		600	700	800	600	700	800	600	700	800	600	700	800
Catalyst		B	A		B	A		B	A		B	A	
Reduced by Hydrogen	1	1.02	0.89	0.96	0.21	0.18	0.21	61.09	60.94	61.92	10.80	9.51	10.50
Auto-reduced	2	1.01	0.90	1.00	0.22	0.19	0.21	61.79	61.86	61.55	10.98	9.80	10.72
	3	1.01	0.94	1.01	0.21	0.20	0.24	61.49	61.55	62.87	10.86	10.11	11.48
	4	1.01	1.00	1.06	0.21	0.21	0.23	61.35	61.46	61.74	10.77	10.80	11.63
	5	0.99	1.05	1.07	0.22	0.22	0.23	61.86	61.58	61.66	10.85	11.31	11.64
Equilibrium values		1.00			0.24			63.01			11.47		

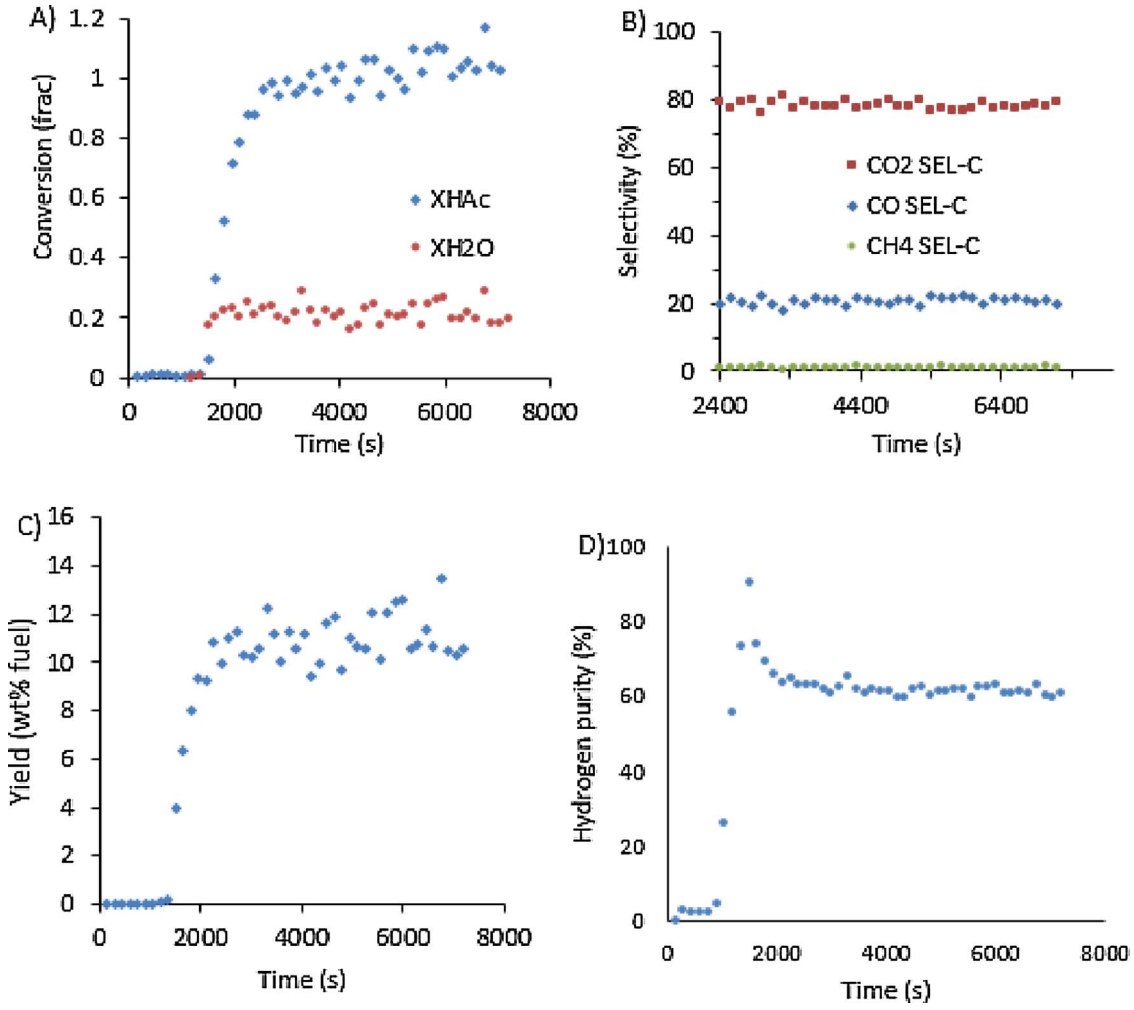

Fig. 4. A) Conversion fraction, B) selectivity to C gases, C) hydrogen yield D) hydrogen purity (T_{SR} = 600 °C, T_{OX} = 700 °C, cycle 2, Catalyst A, WHSV set to 2.36 h^{-1}, and S/C = 3).

Table 4
Solid carbon (CHN elemental analysis) on catalysts A and B at different oxidation temperatures (T_{SR} = 600 °C, WHSV = 2.36 h^{-1}, S/C = 3), duration of reforming experiments: 2 h in all cases).

Catalyst, final state, cycle number	T_{OX} (°C)	$C_{(S)}$ on catalyst (mol)	$C_{(S)}$ on catalyst (mol% of feed C of individual cycle)
Used catalyst B, oxidised, 5 cycles	600	3.57×10^{-4}	0.52
Used catalyst A, oxidised, 5 cycles	600	8.32×10^{-4}	1.22
Used catalyst A, oxidised, 5 cycles	700	3.65×10^{-4}	0.54
Used catalyst A, oxidised, 5 cycles	800	2.68×10^{-4}	0.39
Used catalyst B, reduced, 5 cycles	800	55.6×10^{-4}	8.15
Used catalyst A, reduced, 5 cycles	800	79.1×10^{-4}	11.6

Table 5
BET surface analysis of fresh and used catalyst for CLSR process (S/C = 3, T_{SR} = 600 °C, WHSV = 2.5 h^{-1}).

	MBET surface area (m^2/g)	Pore volume (cc/g)	Pore radius (nm)
Fresh Catalyst B (oxidised form)	34.9	0.068	1.9
H_2-Reduced fresh catalyst	28.8	0.114	2.4
Used oxidised Catalyst B (oxidised at 600 °C after 1 cycle)	20.9	0.084	1.9
Used oxidised catalyst B (oxidised at 800 °C after 1 cycle)	8.6	0.058	1.9
Used reduced Catalyst after 5 cycles of CLSR with oxidation carried out at 600 °C	26.5	0.131	1.9
Used reduced Catalyst after 5 cycles of CLSR with oxidation carried out at 800 °C	13.9	0.072	1.9

surface area and an increase in porosity was observed during catalyst activation and reduction using hydrogen. Nevertheless, comparison of the used reduced catalyst after several cycles indicates a higher surface area and pore volume in the reduced used catalysts when compared to the used oxidised catalyst.

In regards to oxidation of the catalysts, it was observed that the effect of sintering during oxidation is dependent on the temperature of oxidation; higher temperature of oxidation leads to higher level of sintering and a further loss in surface area and open porosity, as observed in Table 5. It can be postulated that two major phases of surface area changes would occur during the oxidation step, an increase of surface area and porosity would be achieved due to the opening of pores blocked by carbon deposition from the subsequent reforming step, followed by a more pronounced reduction of porosity due to the oxidation of Ni to NiO and resulting sintering particularly at higher oxidation temperature. It is nevertheless reported that the overall surface area and porosity of the chemical looping catalyst is expected to stabilise due to the Red-Ox cycle of chemical looping reforming [23].

It is important to note, the consistent and stable profile with time on

stream observed in the CLSR using catalyst B even after oxidation is carried out at 600 °C (Fig. 2) means that acetic acid decomposition to solid carbon and subsequent carbon gasification reactions are suppressed and minimised due to its non-acidic support and higher surface area compared to catalyst A. As already discussed, acidic supports increase the chances of sintering, cracking reactions, thermal decomposition and other polymerisation reactions which would naturally result to more graphitic carbon deposition and eventually the deactivation of the catalyst [21,40]. The graphitic carbon deposited on the acidic sites of the support of the steam reforming catalyst would be more prominent in the reforming of feedstocks susceptible to coking and thermal decomposition like acetic acid. Oxidation of the carbon formed would be more difficult when compared to those formed on the surface of the catalyst. As seen in the case of catalyst A, this could be improved by the increase in the temperature of oxidation.

3.3. Optimised chemical looping cycling stability for catalyst B at T_{SR} 650 °C and T_{OX} 800 °C

Ten CLSR cycles were conducted at 650 °C (T_{SR}) using catalyst B, which, as promoted in the previous section, is a more effective chemical looping reforming catalyst of acetic acid when compared to catalyst A; these were done at a WHSV of 2.5 h^{-1} and T_{OX} set to 800 °C.

3.3.1. Gas outputs in CLSR cycling stability study

A similar product gas profile as identified in Fig. 2 with hydrogen, CO, CO_2 and CH_4 as the main product was observed in all CLSR runs, while in the oxidation run O_2, CO and CO_2 were the major products. Table 6 shows the results derived from elemental analysis during the fuel on feed stage; the conversion fraction (X_{HAc} and X_{H2O}) calculated using Eqs. (1A) and (1B), hydrogen yield (wt.%) calculated using Eq. (2) and hydrogen purity (%) calculated using Eq. (3) were consistent over the 10 cycles of CLSR, these indicated no obvious loss in the catalyst activity down to coking or catalyst deactivation. The minimum water conversion efficiency when compared to equilibrium was 83% with the maximum efficiency at the 9th reforming cycle of 92% when compared to equilibrium values. The water conversion fraction increased as the fuel conversion increased, but no obvious trend which might indicate catalyst deterioration was observed in all 10 CLSR cycles; this entails that stable steam reforming with high affinity towards the production of hydrogen was apparent in all 10 CLSR cycles. The 'space time hydrogen yield', calculated as the moles of hydrogen produced per unit mass of catalyst and per unit time was also calculated and shown in Table 6. The catalysts auto-reduced by acetic acid performed favourably ($X_{HAc} > 0.94$) when compared with the H_2-reduced catalyst.

This is similar to previous studies on chemical looping steam reforming of pyrolysis oils, which concluded that auto-reduction of acetic acid and subsequent reforming of acetic acid and pyrolysis oil can be done efficiently without obvious deterioration in its feedstock conversion [28,30].

The hydrogen yield (wt.%) and the purity of hydrogen (% dry basis) produced also showed high stability across all cycles; the efficiency of the yield across all 10 cycles of chemical looping reforming was between 89% and 97% when compared to equilibrium, and 77% and 85% when compared to theoretical maximum. The trend in the hydrogen yield also corresponds to the fuel conversion (X_{HAc}) of the reducing-steam reforming stage. The hydrogen purity (%) was also consistent across all 10 cycles in the reducing phase with an efficiency of 93% observed across all cycles when compared to equilibrium calculations, this is equivalent to 98% compared to theoretical maximum or stoichiometric values.

As seen in Table 7, the selectivity to hydrogen containing gases ($SelH_{2,H_2}$ and $SelCH_{4,H_2}$) shows no disparity across all 10 reforming cycles. CH_4 is an intermediate by-product formed from methanation reactions (prominent at lower temperatures) and homogenous cracking of acetic acid which is promoted on nickel catalysts due to its high affinity towards breaking C—C bonds [45–47]; its decomposition has been attributed as one of the major routes of catalyst deactivation for the steam reforming of acetic acid [48]. The Sel CH_{4,H_2} is primarily determined by the S/C, catalyst loading and T_{SR}; nevertheless, high selectivity to methane ranging from 4% to ca15% has been reported in previous studies on nickel catalysts [49,50]. The obtained Sel CH_{4,H_2} and Sel H_{2,H_2} in this study are relatively close to equilibrium values and consistent across all 10 cycles of CLSR. This strongly indicate, the rate of reaction of the process is primarily determined by the thermodynamics of the reaction system. It also indicates, no loss of activity in the efficiency of the reforming catalyst towards efficient steam reforming and hydrogen production across all 10 cycles of CLSR. In regards to selectivity to C-gases, there is no major change identified for selectivity to $CH_{4,C}$.The selectivity to CO_2 increased sparingly from the

Table 7
Selectivity to C-gases and H-gases across 10 cycles (T_{SR} = 650 °C, T_{OX} = 800 °C, catalyst B, WHSV = 2.5 h^{-1}, S/C = 3).

		Selectivity to C-gases (Eq. (4))			Selectivity to H-gases (Eq. (5))	
	Cycle	Sel $CO_{2,C}$	Sel $CO_{,C}$	Sel $CH_{4,C}$	Sel $H_{2,H2}$	Sel $CH_{4,H2}$
H_2-Reduced Auto reduced	1	75.9	23.5	0.6	99.6	0.4
	2	77.6	21.8	0.7	99.6	0.4
	3	77.5	22.0	0.5	99.7	0.3
	4	78.5	20.9	0.5	99.7	0.3
	5	78.4	21.1	0.5	99.7	0.3
	6	77.8	21.7	0.5	99.7	0.3
	7	78.4	21.2	0.4	99.7	0.3
	8	78.2	21.4	0.4	99.8	0.2
	9	78.1	21.4	0.5	99.7	0.3
	10	78.2	21.4	0.5	99.7	0.3
	Equilibrium	72.8	26.8	0.4	99.5	0.5

Table 6
Acetic acid and water conversion Fractions, hydrogen purity and hydrogen yield (wt.%) (T_{SR} = 650 °C, T_{OX} = 800 °C, catalyst B, WHSV = 2.5 h^{-1}, S/C = 3).

	Cycle	X_{HAc} (Eqs. (1A) and (1B))	X_{H2O}	Hydrogen purity (%) (Eq. (3))	Hydrogen yield (wt.%) (Eq. (2))	Space time yield (mol kg_{cat}^{-1} h^{-1})
H_2-Reduced Auto-reduced	1	1.00	0.21	61.77	10.92	27.75
	2	0.95	0.20	61.71	10.31	26.20
	3	0.98	0.20	61.63	10.56	26.85
	4	0.98	0.21	62.04	10.75	27.30
	5	0.97	0.20	61.73	10.52	26.75
	6	0.98	0.20	61.69	10.63	27.00
	7	0.96	0.21	61.99	10.51	26.70
	8	0.95	0.20	61.87	10.40	26.40
	9	1.05	0.22	61.88	11.38	28.95
	10	1.03	0.22	61.90	11.23	28.55
	Equilibrium	1.00	0.24	63.14	11.53	

first cycle (H_2-reduced catalyst) to the subsequent cycles; this also corresponded to a decrease in the selectivity to CO from the first cycle to subsequent cycles, for the auto-reduced catalyst. This observation coupled with the stable water conversion fraction indicates improved water gas shift in the reducing-steam reforming stage and could also indicate less carbon gasification.

3.3.2. Solid carbon product in redox cycling stability study

Post experimental analysis on the used chemical looping reforming catalyst and condensates samples collected over 10 cycles were also conducted; the possibility of leaching of nickel catalyst has been postulated for steam reforming of acetic acid [30], hence to check the extent of leaching, ICP-MS testing was carried out on the condensate collected after the 10th chemical looping cycle. 0.0819 mg/l of nickel was detected through ICP-MS, which indicated potential leaching of the catalyst into the condensate, these however corresponded to about 0.0001% of the nickel originally present in the catalyst and is therefore taken as insignificant. Total organic carbon analysis of the condensates collected after the reducing-steam reforming phase of the CLSR experimental runs using catalyst B indicates there was no obvious trend or relationship across the cycles. The carbon (mol) found in the condensate constituted less than 0.1% of all carbon formed for each experimental run with the majority share of carbon formed either present in the product gas as CO_2, CO and CH_4 formed during oxidation or auto-reduction/reforming or deposited as solid on the catalyst.

TGA-FTIR analysis was conducted on the used, reduced, CLSR catalyst after 10 cycles of chemical looping steam reforming cycles. The evolution of CO_2 from the FTIR chemigram was plotted against the weight loss of catalyst from the TGA (Fig. 5); Two CO_2 peaks were observed in the Chemigram profile [30,48]; this indicates that two forms of carbon were formed. Previous studies indicate that the CO_2 generated at the lower temperature (360 °C) was due to coking on the active sites of the surface of the catalyst while the other type of carbon formed (544 °C) was pseudo-graphitic in structure and contains poly aromatic compounds. These are most likely formed in and on the catalyst support or in some cases at the interface between the catalyst supports and the active sites [21,30,51,52].

3.3.3. Catalysts characteristics after CLSR-HAc use in redox stability study

SEM images of the used CLSR catalyst (Fig. 6) shows the presence of filamentous carbon; in higher magnification, it is observed that two types of carbon filaments were formed in regards to size of the carbon filaments. Denser and larger carbon filaments with a diameter of 51 nm were identified, and shorter and smaller filaments with diameter between 14 nm and 18 nm which formed the major share of carbon filaments were also observed. It has been suggested in a previous study that the size of the carbon filaments formed on the surface of the catalyst might have an effect on the process efficiency [30]; the presence of more dense or larger carbon filaments would make it more difficult for the fuel and steam reacting molecules to reach the active sites of the catalyst thus introducing a larger external mass transfer barrier and hence reducing the rate of reaction and catalytic activity. The oxidation of shorter and smaller carbon filaments which are prominent on catalyst B is also easier when compared to oxidation of larger and denser carbon filaments.

TEM images and SAED diffraction patterns of the used CLSR catalyst can be seen in Fig. 7; the images in Fig. 7(A) and the diffraction pattern in Fig. 7(B) indicate and confirm the presence of amorphous carbon across the catalyst; these carbon spots are not evenly distributed across the catalyst but are dispersed. The different intensity in the colours also indicates, the level of carbon deposition varies across different point of the catalyst. A poly-crystalline structure Fig. 7(C, D) was also observed in higher magnification of the catalyst which as expected represents the pseudo graphitic carbon formed as already reported for the steam reforming of acetic acid [30].

The poly crystalline structure as observed in the SAED diffraction patterns (Fig. 7D) corresponds to CO_2 peak observed at higher temperatures in the chemigram obtained from TGA-FTIR analysis as detailed in Fig. 5 while the amorphous carbon corresponds to the carbon filaments as observed in SEM images (Fig. 6) and the lower CO_2 peak in the TGA-FTIR chemigram (Fig. 5).

4. Conclusion

An experimental study was performed using two conventional nickel based catalysts in a packed bed reactor to study the possibility and efficiency of chemical looping steam reforming of acetic acid, as a model compound of pyrolysis oils. The following observations and inferences were deduced after post experimental analysis;

- The temperature at which the catalyst is oxidised in the air feed/oxidation step plays a vital role in chemical looping steam reforming; this is however dependent on the type of catalyst utilised;
- Acetic acid is thermally unstable and decomposes easily; however, chemical looping steam reforming process can be sustained at the right operating conditions as gasification of carbon deposited occurs as the reaction goes on
- The auto reduction of the oxidised catalyst by acetic acid in an

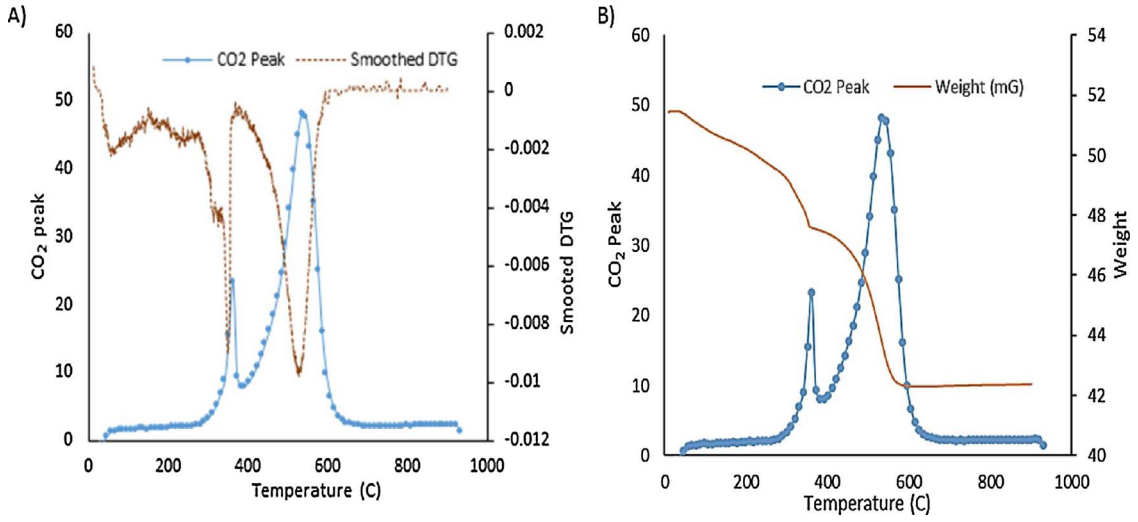

Fig. 5. TGA FTIR analysis of used CLSR catalyst B (reduced form) A) CO_2 against smoothed DTG B) CO_2 against weight loss of catalyst (T_{SR} = 650 °C, T_{OX} = 800 °C, S/C = 3 and WHSV = 2.36 h^{-1}).

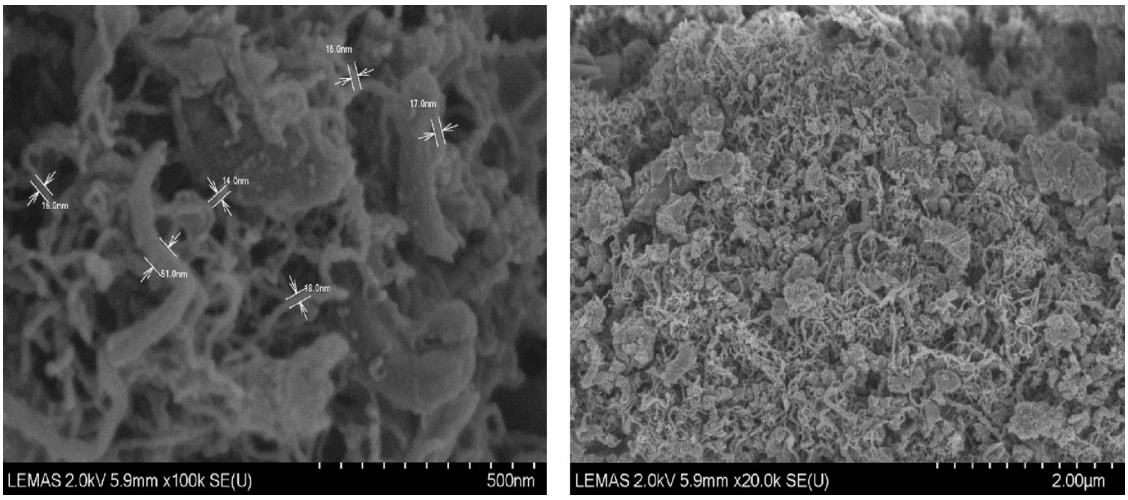

Fig. 6. SEM images of the Used CLSR catalyst B after 10 cycles (in reduced form) T_{SR} = 650 °C, T_{OX} = 800 °C, catalyst B, WHSV = 2.5 h^{-1}, S/C = 3.

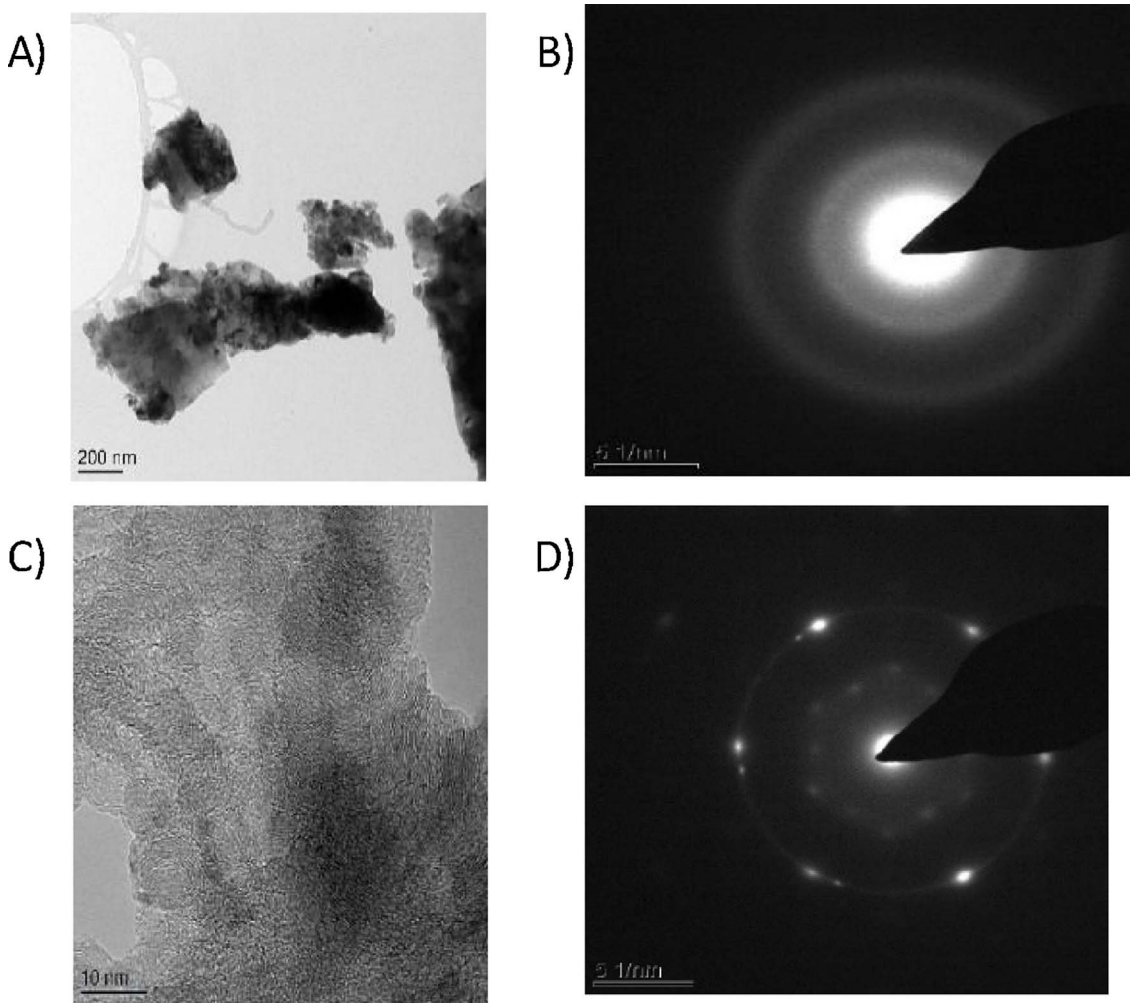

Fig. 7. TEM images and Diffraction patterns of used chemical looping steam reforming catalysts (in reduced form) after 10 cycles of reforming; T_{SR} = 650 °C, T_{OX} = 800 °C, catalyst B, WHSV = 2.5 h^{-1}, S/C = 3.

integrated system can be sustained across several cycles at the operating conditions set for this study;

- An overall carbon balance also indicated that in the overall cyclic process, the majority of the carbon from the feedstock is converted efficiently to the product gas with no apparent loss of activity in the cycles.

It can then be concluded that chemical looping steam reforming of acetic acid can be carried out successfully and efficiently with a high fuel conversion and hydrogen yield across several cycles at a stable and sustainable rate as long as the operating parameters in regards to catalyst type, reforming and oxidising temperature, and steam to carbon ratio are taken into account.

Acknowledgements

The authors would like to acknowledge the Niger Delta Development Commission (NDDC) Nigeria for financial support. Martyn V. Twigg at TST Limited is gratefully acknowledged for providing the nickel catalysts. We also thank the UKCCSRC EPSRC consortium (EP/G01244X/1) for call to grant "SUPERGEN: Delivery of Sustainable Hydrogen". Data associated with this paper can be found at https://doi.org/10.5518/309.

References

[1] PATH, Annual Report on World Progress in Hydrogen, Partnership for Advancing the Transition to Hydrogen (PATH), Washington, D.C, 2011.
[2] D.B. Levin, R. Chahine, Int. J. Hydrogen Energy 35 (2010) 4962–4969.
[3] J. Ritter, A. Ebner, Report for US Department of Energy, (2005).
[4] R. Navarro, M. Sanchez-Sanchez, M. Alvarez-Galvan, F. Del Valle, J. Fierro, Energy Environ. Sci. 2 (2009) 35–54.
[5] C. Zygarlicke, Renewable Hydrogen: Biomass for Sustainable Hydrogen Transportation Fuel, Biomass Magazine, BBI International, Grand Forks, 2014.
[6] T.A. Milne, C.C. Elam, R.J. Evans, Hydrogen from Biomass: State of the Art and Research Challenges, International Energy Agency, USA, 2001.
[7] M. Balat, Energy Sources Part A 31 (2009) 516–526.
[8] X. Hu, G. Lu, Appl. Catal. B: Environ. 88 (2009) 376–385.
[9] D. Wang, D. Montane, E. Chornet, Appl. Catal. A: Gen. 143 (1996) 245–270.
[10] C. Rioche, S. Kulkarni, F.C. Meunier, J.P. Breen, R. Burch, Appl. Catal. B: Environ. 61 (2005) 130–139.
[11] F. Bimbela, M. Oliva, J. Ruiz, L. García, J. Arauzo, J. Anal. Appl. Pyrolysis 85 (2009) 204–213.
[12] F. Bimbela, M. Oliva, J. Ruiz, L. García, J. Arauzo, J. Anal. Appl. Pyrolysis 79 (2007) 112–120.
[13] S. Czernik, R. French, C. Feik, E. Chornet, Ind. Eng. Chem. Res. 41 (2002) 4209–4215.
[14] S. Czernik, R. French, C. Feik, E. Chornet, Production of Hydrogen from Biomass-Derived Liquids, DOE Hydrogen Program Review, 2001.
[15] R.M. Zin, Advanced Steam Reforming of Pyrolysis Oils and Their Aqueous Phase, School of Process, Environmnetal and Materials Engineering, University of Leeds, Energy and Research Institute, 2012.
[16] K. Sipilä, E. Kuoppala, L. Fagernäs, A. Oasmaa, Biomass Bioenergy 14 (1998) 103–113.
[17] P. Pimenidou, V. Dupont, Bioresour. Technol. 109 (2012) 198–205.
[18] X. Hu, G. Lu, Appl. Catal. B: Environ. 99 (2010) 289–297.
[19] K. Takanabe, K.-i. Aika, K. Seshan, L. Lefferts, J. Catal. 227 (2004) 101–108.
[20] K. Takanabe, K.-I. Aika, K. Seshan, L. Lefferts, Chem. Eng. J. 120 (2006) 133–137.
[21] A. Basagiannis, X. Verykios, Appl. Catal. A: Gen. 308 (2006) 182–193.
[22] V. Dupont, A. Ross, I. Hanley, M. Twigg, Int. J. Hydrogen Energy 32 (2007) 67–79.
[23] B. Jiang, B. Dou, Y. Song, C. Zhang, B. Du, H. Chen, C. Wang, Y. Xu, Chem. Eng. J. 280 (2015) 459–467.
[24] Q. Zafar, T. Mattisson, B. Gevert, Ind. Eng. Chem. Res. 44 (2005) 3485–3496.
[25] T. Hoang, B. Geerdink, J. Sturm, L. Lefferts, K. Seshan, Appl. Catal. B: Environ. 163 (2015) 74–82.
[26] N. Giannakeas, A. Lea-Langton, V. Dupont, M.V. Twigg, Appl. Catal. B: Environ. 126 (2012) 249–257.
[27] R.M. Zin, A. Ross, J. Jones, V. Dupont, Bioresour. Technol. 176 (2015) 257–266.
[28] A. Lea-Langton, R.M. Zin, V. Dupont, M.V. Twigg, Int. J. Hydrogen Energy 37 (2012) 2037–2043.
[29] J. Fermoso, M.V. Gil, F. Rubiera, D. Chen, ChemSusChem 7 (2014) 3063–3077.
[30] F. Cheng, V. Dupont, Int. J. Hydrogen Energy 38 (2013) 15160–15172.
[31] P.N. Kechagiopoulos, S.S. Voutetakis, A.A. Lemonidou, I.A. Vasalos, Energy Fuels 20 (2006) 2155–2163.
[32] E.C. Vagia, A.A. Lemonidou, Appl. Catal. A: Gen. 351 (2008) 111–121.
[33] R.M. Zin, A. Lea-Langton, V. Dupont, M.V. Twigg, Int. J. Hydrogen Energy 37 (2012) 10627–10638.
[34] F. Cheng, V. Dupont, M.V. Twigg, Appl. Catal. B: Environ. 200 (2017) 121–132.
[35] P. Pimenidou, G. Rickett, V. Dupont, M. Twigg, Bioresour. Technol. 101 (2010) 6389–6397.
[36] S. Gordon, B.J. McBride, Computer Program for Calculation of Complex Chemical Equilibrium Compositions and Applications, National Aeronautics and Space Administration, Office of Management, Scientific and Technical Information Program, 1996.
[37] A.A. Lemonidou, E.C. Vagia, J.A. Lercher, ACS Catal. 3 (2013) 1919–1928.
[38] M.N. Khan, T. Shamim, Energy Procedia 61 (2014) 2034–2037.
[39] P. Pimenidou, Novel Process of Hydrogen Production from Liquids of Biomass Origin, School of Process, Environmmental and Material Engineering, University of Leeds, 2010.
[40] A. Basagiannis, X. Verykios, Int. J. Hydrogen Energy 32 (2007) 3343–3355.
[41] S. Goicoechea, E. Kraleva, S. Sokolov, M. Schneider, M.-M. Pohl, N. Kockmann, H. Ehrich, Appl. Catal. A: Gen. 514 (2016) 182–191.
[42] J.d.S. Lisboa, D.C. Santos, F.B. Passos, F.B. Noronha, Catal. Today 101 (2005) 15–21.
[43] K. Kousi, N. Chourdakis, H. Matralis, D. Kontarides, C. Papadopoulou, X. Verykios, Appl. Catal. A: Gen. 518 (2016) 129–141.
[44] V. Nichele, M. Signoretto, F. Pinna, F. Menegazzo, I. Rossetti, G. Cruciani, G. Cerrato, A. Di Michele, Appl. Catal. B: Environ. 150 (2014) 12–20.
[45] J. Sinfelt, Adv. Catal. 23 (1973) 91–119.
[46] R. Davda, J. Shabaker, G. Huber, R. Cortright, J.A. Dumesic, Appl. Catal. B: Environ. 43 (2003) 13–26.
[47] Stefanie C.M. Mizuno, Adriano H. Braga, Carla E. Hori, João Batista O. Santos, José Maria C. Bueno, Steam reforming of acetic acid over $MgAl_2O_4$-supported Co and Ni catalysts: effect of the composition of Ni/Co and reactants on reaction pathways, Catalysis Today (2017).
[48] W. Nabgan, T.A.T. Abdullah, R. Mat, B. Nabgan, A.A. Jalil, L. Firmansyah, S. Triwahyono, Int. J. Hydrogen Energy 42 (2017) 8975–8985.
[49] Z. Li, X. Hu, L. Zhang, S. Liu, G. Lu, Appl. Catal. A: Gen. 417 (2012) 281–289.
[50] S. Thaicharoensutcharittham, V. Meeyoo, B. Kitiyanan, P. Rangsunvigit, T. Rirksomboon, Catal. Today 164 (2011) 257–261.
[51] D. Duprez, M. Demicheli, P. Marecot, J. Barbier, O. Ferretti, E. Ponzi, J. Catal. 124 (1990) 324–335.
[52] J. Barbier, Appl. Catal. 23 (1986) 225–243.